Experimental investigation of the usability of the rifled serpentine tube to improve energy and exergy performances of a nanofluid-based photovoltaic/thermal system

A. Shahsavar, P. Jha, M. Arici, Patrice Estellé

Experimental investigation of the usability of the rifled serpentine tube to improve energy and exergy performances of a nanofluid-based photovoltaic/thermal system

Amin Shahsavar[1], Prabhakar Jha[2], Muslum Arici[3], Patrice Estellé[4]

[1]Department of Mechanical Engineering, Kermanshah University of Technology, Kermanshah, Iran

[2]Department of Mechanical Engineering, National Institute of Technology Silchar, Assam 788010, India

[3]Mechanical Engineering Department, Engineering Faculty, Kocaeli University, Turkey

[4] Univ Rennes, LGCGM, F–35000 Rennes, France

* Corresponding author

Emails:

patrice.estelle@univ-rennes1.fr

Credit author statement

Amin Shahsavar: Conceptualization, Performing the experiments, Reviewing and Editing. **Prabhakar Jha**: Data curation, Writing- Original draft preparation. **Muslum Arici**: Writing- Reviewing and Editing. **Patrice Estellé**: Supervision, Reviewing and Editing.

Experimental investigation of the usability of the rifled serpentine tube to improve energy and exergy performances of a nanofluid-based photovoltaic/thermal system

Amin Shahsavar[1], Prabhakar Jha[2], Muslum Arici[3], Patrice Estellé[4]

[1]Department of Mechanical Engineering, Kermanshah University of Technology, Kermanshah, Iran

[2]Department of Mechanical Engineering, National Institute of Technology Silchar, Assam 788010, India

[3]Mechanical Engineering Department, Engineering Faculty, Kocaeli University, Turkey

[4] Univ Rennes, LGCGM, F–35000 Rennes, France

* Corresponding author

Emails:

patrice.estelle@univ-rennes1.fr

Abstract

This experimental study aims to energetically and exergetically compare the performance of a PVT system with sheet-and-plain serpentine tube collector (base PVT system) with two cases of modified PVT systems. The modified PVT systems are the replacements of plain serpentine tube with rifled serpentine tube with 3 ribs (3-start rifled PVT system) and 6 ribs (6-start rifled PVT system). The electrical parameter of the PV module without cooling is compared with the three cases of the PVT system with cooling. The cooling fluid is water/magnetite nanofluid. The effect of nanofluid flow rates (20-80 kg/hr) and nanoadditive volume concentrations (0-2%) over the three cases of the PVT system is investigated to propose a suitable combination of flow rate and NA concentration offering the best energetic and exergetic performances. Thus, the 6-start rifled PVT system achieved a maximum of

22.5% and 3.8% higher overall energy efficiency, and 5.9%, and 1.9% higher overall exergy efficiency than the base and 3-start rifled PVT systems at flow rate and concentration of 80 kg/hr and 2%. Finally, the electrical power generated by the base, 3-start rifled, and 6-start rifled PVT systems achieved maximum enhancement of 27.5%, 29.5%, and 31.5% compare to the PV module without cooling.

Keywords: PVT system; rifled serpentine tubes; nanofluid; concentrations; energy efficiency; exergy efficiency.

1. Introduction

As reported by scientists, non-renewable energy sources will be exhausted by the end of the 22nd century [1]. Hence, significant attention is paid to renewable energy sources and development of renewable energy systems. Solar energy is one such renewable energy source that is extensively used to meet energy demand [2]. The conversion technologies of solar energy have been assiduously investigated and noteworthy advances in recent decades have been carried out in this area, including photovoltaic (PV), photochemical, photothermal, and photovoltaic-thermal (PVT) systems as a third-generation solar systems. The defining feature of all these collectors, that differentiates them from other solar systems, is perhaps the cogeneration of heat and electricity [3]. PV system is one such kind of solar-based power generation unit. In the PV system, the production of electricity is realized due to the falling of sunlight on the semi conductive materials (silicon). These semi conductive silicon materials are referred to as solar or PV cells in the field of PV technology [4]. The electricity generation is the result of potential difference across the negative and positive poles that actuates the flow of electrons. But, the exposed PV cells to the scorching heat from the sun leads to a high PV module operating temperature. The high operating temperature of the PV

module deteriorates the PV electrical efficiency [5]. To overcome the demerit of the PV module, the thermal collector was conceptualized in 1976 by Wolf [6] and termed as a photovoltaic thermal (PVT) collector system. In a physical form, the PVT system has a thermal collector placed below the PV module. The thermal collector has a fluid channel that enables the fluid to flow through the back surface of the PV module and results in withdrawing the unutilized heat present in the PV module's surface [7]. This heat withdrawal leads to improved PV electrical efficiency and simultaneously provides thermal energy. The thermal energy received is employed for low heat applications like industrial and domestic applications [8].

Since the technological evolution of the PVT system, a never-ending attempt is in the process to amplify its efficacy in terms of both thermal and electrical energies. Many pieces of research have explored the possibilities of improving the overall efficiency of air and water-based PVT systems by employing techniques such as optimization of design parameters [9-10], inclusion of heat exchanger in flow channel [11-14], flow configurations [15,16], glazing/unglazing [17, 18], etc. Apart from air, and water, some other conventional fluids are used as coolants for the PVT system such as ethylene glycol and motor oil. These conventional fluids are also termed as another significant parameter to withdraw heat from the flow channel. Motor oil and ethylene glycol are associated with higher cost and lower economic benefit. Nanofluids are a promising option as cooling fluids because they possess superior thermal properties over ordinary fluids [20-24].

The suitability of a nanofluid as a cooling fluid in PVT systems has been explored by many scientists in recent years. Yazdanifard et al. [25] tested the PVT system under the laminar and turbulent flow for two different nanofluids. This work has shown that the addition of NAs increases the overall efficiency which is more dominant for turbulent flow rather than laminar flow. The investigation further indicated that for a turbulent flow, energy, and exergy

generated from the PVT system were higher for a higher NA diameter, while for laminar flow, an opposite behavior was witnessed. Again, it was revealed that the aluminum oxide (Al_2O_3) nanofluid has a higher efficiency than the titanium oxide (TiO_2) nanofluid. Moradgholi et al. [26] reported an experimental study using methanol mixed Al_2O_3 nanofluid. The study showed that the use of Al_2O_3/methanol nanofluid decreases the PV module temperature by 14.5°C which simultaneously generated 1.4 W higher power output. A sheet and tube-based PVT system with Al_2O_3/water, ZnO/water, and TiO_2/water nanofluids were numerically studied by Sardarabadi and Passandideh-Fard [27]. This research evidenced that the thermal performance of the PVT system is better when it is operated with ZnO/water nanofluid whereas the better electrical performance is imparted by the Al_2O_3/water nanofluid. Purohit et al. [28] numerically investigated a combination of water and alumina as a nanofluid for the PVT system and compared with the water-based PVT system in terms of working performance. They reported a 25% enhancement in overall working performance for the nanofluid-based PVT system as compared to the water-based PVT system. However, this study also revealed that at the same pumping power, this percentage enhancement falls to 13.8% for the water-based PVT system compared to the nanofluid-based PVT system. Al-Waeli et al. [29] studied a nanofluid (SiC/water)-based PVT system. The prepared nanofluid was introduced into the phase change material (PCM) tank to check its effect on the PV module temperature. It was found that the PV module temperature reduced considerably. Another concept of PCM was implemented by Hassan et al. [30] where a hybrid PCM based nanofluid was used as a coolant for the PVT system. It was shown that the used nanofluid enhances the system's electrical efficiency by 23.9% when compared with the water-based PVT system. A techno-economic study was experimentally carried out by Al-Waeli et al. [31] where a paraffin mixed nano-SiC nanofluid was made to pass through the backside of the PV module. The study reported that this modification improved the electrical efficiency

from 7.1 to 13.7%, as well as provided 72% thermal efficiency. On the other hand, the techno-economic section of the study suggested the payback period and electricity cost as 5-6 years and 0.125 $/kWh. A new theoretical approach was established by Fudholi et al. [32] to evaluate the performance of nanofluid-based PVT system. In this study, an aqueous suspension of TiO_2 was utilized as NA for the nanofluid preparation. The findings reported a 13-25% augmentation in the energy efficiency of the PVT system due to the utilization of NAs in comparison to pure water.

Exergy and entropy are the two important concepts in the thermodynamical systems, the former shows the system's ability to execute useful work whilst the latter indicates the system's inability to execute useful work [33]. The important concept of exergy is used in nanofluid-based PVT system also by various researchers [34-38]. Sardarabadi et al. [34] experimentally investigated the performance of nanofluid SiC/water nanofluid in PVT system. The authors reported the exergy efficiency of pure water (19.36%) increased to 22.61% and 24.31% for 1 wt% and 3 wt% of SiC nanoparticles, respectively. Ag/water nanofluid with 4 wt% in nanoparticle content was studied and compared with the traditional PVT system by Aberoumand et al. [35]. They concluded that the PVT system's exergy efficiency and electrical power was enhanced by 30% and 10%, respectively, with nanofluid over the traditional PVT system. Another study to improve the PVT system's exergy efficiency was performed by Hosseinzadeh et al. [36]. For this purpose, they used a combination of nanofluid (ZnO/water) and PCM (paraffin wax), which resulted in an attainment of 13.6% of overall exergy efficiency. With a similar objective of improving the exergy performance, a microencapsulated PCM slurry was used as a cooling fluid by Yu et al. [37]. In their study, the exergy performance was mapped with the variation of the melting point and slurry concentration. It was found that the increase in melting point and slurry concentration increased the exergy efficiency. Khanjari et al. [38] investigated a PVT system

with two different nanofluids, Ag/water and Al/water varying NA concentration. It was shown that the higher NA concentration results in higher heat transfer properties for both nanofluids. On the other hand, Ag/water nanofluid resulted in a better PVT system's exergy efficiency as compared to the alumina/water nanofluid for the same NA concentration.

As reported before, some previous works have been conducted to evaluate and improve the energy and exergy generation capacity of the nanofluid-based PVT systems. This is also the objective of the present work to improve the energy and exergy performance of the traditional nanofluid-based PVT system by replacing, in addition, the plain serpentine tube with a rifled serpentine tube. To the best of our knowledge, the energy and exergy analysis of the PVT system with a riffled serpentine tube collector has never been conducted in the past. The effects of nanofluid flow rate (20-80 kg/hr), and NA volume concentration (0-2%) on the energy and exergy performances of the modified PVT systems are studied and compared with that of traditional system. A suitable combination of flow rate and NA concentration that offers the best energetic and exergetic performances is identified.

2. Experimental set-up

The objective of this research is investigate three experimental cases of the PVT system coupled with the use of nanofluids and evaluate the best option based on energy and exergy analysis. The first case is the plain serpentine tube PVT system which is considered as the base case. The other two PVT systems are the modifications of the base PVT system, which is done by replacing a plain serpentine tube with a rifled serpentine tube with 3 ribs (3-start rifled PVT system), and 6 ribs (6-start rifled PVT system).

The dimension considered for the serpentine tube is 8 mm in inner diameter and 2 mm in thickness, and the collector is made of copper. The collector is positioned at the back of the PV module by applying thermal grease while serpentine tubes are attached to the collector

surface with the help of soldering process. To reduce heat loss from the back surface of collector, the serpentine tubes are insulated with stone wool. Both the height and width of ribs used in the 3-start and 6-start rifled PVT system are 0.4 mm, while the rib pitch is 1 mm. The schematic presentation of the considered PVT systems is illustrated in Fig. 1.

(a)

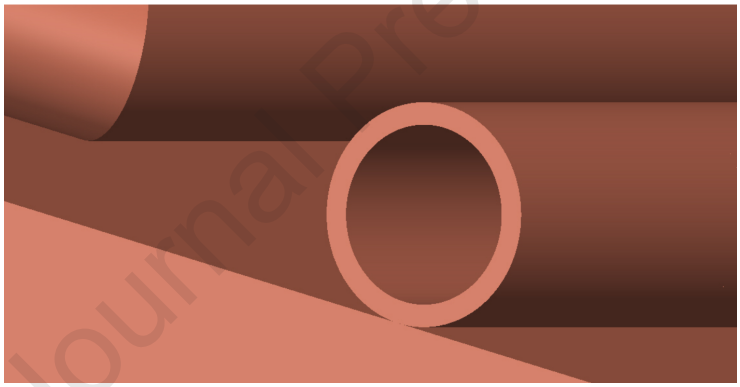

(b)

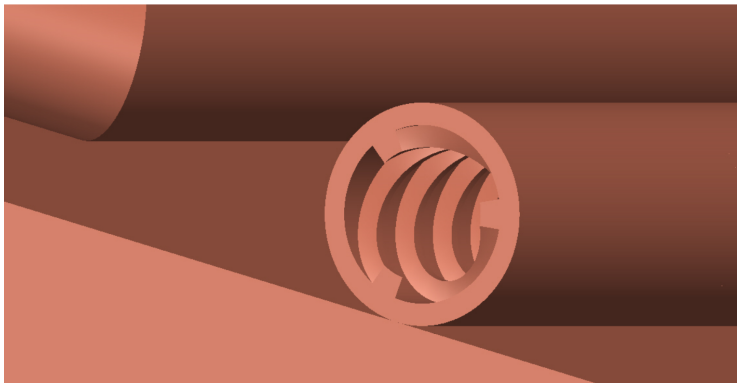

(c)

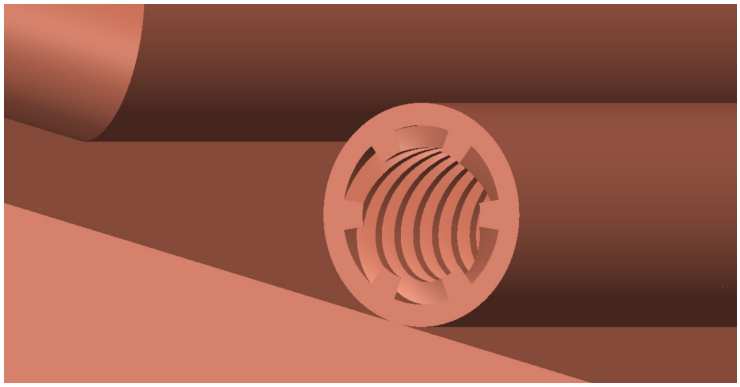

(d)

Fig. 1. Schematic view of the (a) sheet-and-serpentine tube collector, (b) plain serpentine tube, (c) 3-start rifled serpentine tube and (d) 6-start rifled serpentine tube.

As mentioned above, the objective of this work is to compare three cases of the PVT system considering similar input conditions such as radiation intensity and ambient temperature. For such reason, a solar simulator is fabricated to perform the experimental investigation under the laboratory situations. The solar simulator consists of an aluminum box (1 nos.), DC fan (4 nos.), 10 W LED lamps (4 nos.), 400 W reflector-sunlight-dysprosium-lamp (RSDL) also described as metal halide lamp (4 nos.), and an AC phase-cut dimmer (1 no.). The first objective is to achieve a similar radiation intensity (126,582 lux≈1000 W/m^2 [39]) and ambient temperature (22 °C) throughout the experiment which has been measured by a lux meter (BF06-Trotec-type) and a thermocouple (K-type). The PV module (Eco-Worthy type) used for the four cases has a dimension of 32 cm×21.5 cm, a power weightage of 10 W and consists of 72 solar cells. A photograph and important specifications of the PV module are respectively given in Fig. 2(a) and Table 1. The temperature at 20 different locations over the PV module (shown in Fig. 2(b)) is also measured with the help of K type thermocouples. The temperature measurements are recorded by a datalogger (JUMO type). To calculate the electrical energy, the current and voltage imparted by the module during its functioning are measured by a multi-meter (LUTRUN-type). The working fluid used in the present

183 investigation is nanofluid, which requires a pump to push it from the inlet to the outlet of the
184 serpentine tube. The pump operates on a DC source and has a head capacity of 3.5 m. The
185 pump also facilitates different pumping speeds which is another requirement for the present
186 investigation as various mass flow rates are used in the study. The pumping speed is
187 measured by utilizing a rotary flow meter (M10000- Malema). The pressure drop caused by
188 the nanofluid across the surfaces of the tubes at various flow rates is measured by a
189 differential type pressure transmitter (3051CD-Rosemount). The circulation process of the
190 nanofluid takes place in a closed cycle. The nanofluid is placed in a 2L capacity reservoir
191 through which the nanofluid is pumped into the collector with the help of a tube and collects
192 heat from the PV module. This cyclic process continues until steady conditions are achieved.
193 Another criterion in the comparative analysis is to have a constant inlet temperature which is
194 maintained throughout the trial and error method by passing the nanofluid through a plate
195 type heat exchanger. The nanofluid, when passing through the heat exchanger, rejects its heat
196 to a separate coolant (mixture of water and ethylene glycol) prepared through a constant
197 temperature bath. The schematic diagram and real photograph of the utilized experimental
198 setup are respectively shown in Fig. 3(a) and (b). Important specifications of the utilized
199 equipment are also presented in Table 2.
200
201 **Table 1.** Technical characteristics of the studied PVT units in the current investigation [40].

PV solar cell (Under standard test conditions)	
Type	Mono-crystalline silicon
Nominal power output (W)	10
Maximum efficiency (%)	16
Number of cells	72
Fill factor	0.726

Dimensions (mm)	33×18×20
Weight (kg)	0.82
Short circuit current (A)	0.69
Open circuit voltage (V)	20.6
Temperature coefficient of power (%/℃)	-0.47
Temperature range (℃)	-40 to 80
Tempered glass thickness (mm)	3.2

202

203

204 (a)

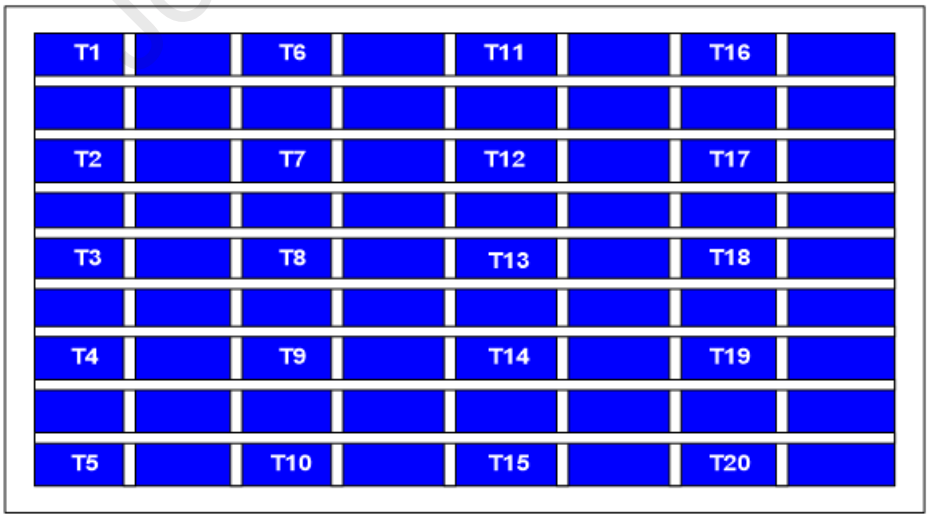

205

206 (b)

207 **Fig. 2.** (a) A photograph of PV module and (b) placement of thermocouples at the front surface of the PV

208 module.

209

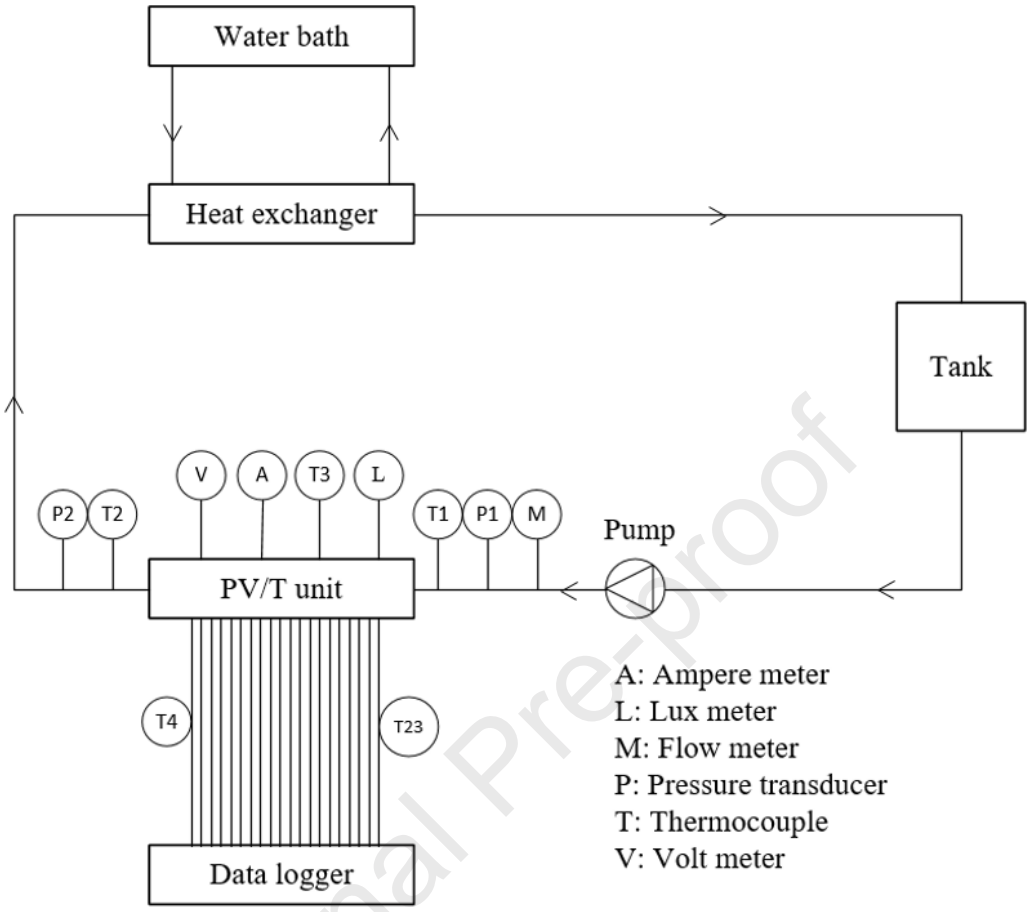

210

211 (a)

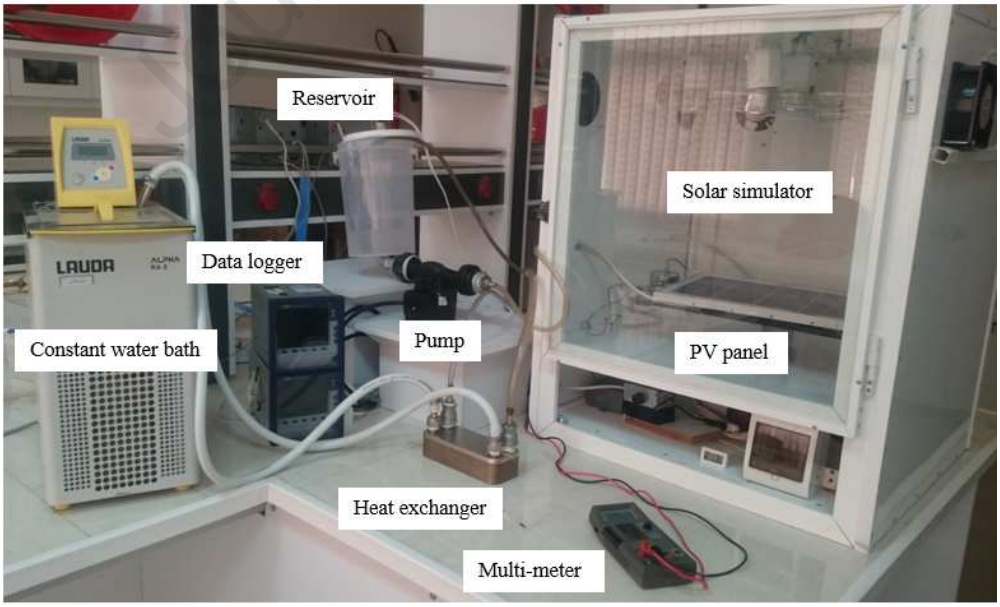

212

213 (b)

214 **Fig. 3.** (a) Physical representation and (b) real photograph of the experimental setup [40].

215

Table 2. The specifications of instrument used in the experimental study [40].

Instrument	Model	Range	Precision (from manufacturer)
Luxmeter	TROTEC-BF06	0-40 klx	±5%±10 lx
Thermometer	K-type	-200–1260 °C	±0.75%
Temperature sensor	TES-1327 K	-150-1260 ℃	±0.1% -1℃
Multimeter DC voltage	LUTURON-DW6060	0-600 V	±0.8%
Multimeter DC current	LUTURON-DW6060	0-10 A	±1%
Rotary flow meter	Malema-M10000	-0.1 to 225 Lit/min	±2%
Pressure transmitter	Rosemount 3051CD	0-2.07 MPa	±1%
Liquid density gravity meter	KEN-DA130N	0-2 g/cm^3	±0.001 g/cm^3
Thermal properties analyzer	Decagon-KD2	0.02-4 W/m.K	±5%

3. Nanofluid preparation and its specification

The co-precipitation method is used to prepare the water/magnetite nanofluid [24] for the present experimental investigation. The different processes associated with the preparation of the water/magnetite nanofluid are:

1. Addition of 67.58 gm of $FeCL_3.6H_2O$ in 100 ml of 2M hydrochloric (HCL) acid.
2. Addition of 39.76 gm of $FeCL_2.4H_2O$ in 100 ml of 2M HCL acid.
3. The compositions obtained in the above processes 1 and 2 are mixed in a ratio of 4 to 1 using a magnetic stirrer for 2 minutes at 100 RPM.
4. 50 mL of 0.7 M ammonia hydroxide under intense stirring is introduced dropwise to the solution obtained in process 3 for 10 min at 700 RPM.
5. The solution obtained in process 4 is placed over the permanent magnet with the help of a container. The permanent magnet discharged the magnetic NA and settled it into the bottom surface of the container.

6. The magnetic particles are added with 8 ml of 25% tetramethylammonium hydroxide and the final solution underwent a centrifugation process for 1 minute at 4000 RPM.
7. The magnetic NAs prepared in the previous step are sufficiently poured into pure water and the resulting solution is stirred using a magnetic stirrer for 30 min at 300 RPM.

All the above-mentioned processes are also presented in a schematic representation in Fig. 4. The stability of the prepared nanofluid samples was investigated using the fact that the instability of the fluid led to the deposition of NAs and, therefore, the change in nanofluid viscosity over time. Therefore, the nanofluid viscosity was measured every day for three weeks by means of a density gravity meter at temperature of 23 ℃ (liquid type, DA-130N, KEN Japan), and the results showed that the viscosity changes were negligible within three weeks. The necessary thermophysical properties of the prepared nanofluid are given in Table 3. Thermal conductivity of NF was measured using a KD2-Pro thermal properties analyzer (Decagon devices, USA) that operates based on the transient hot wire technique. This device has a probe (KS-1) that must be placed in the solution for 90 seconds during the test. To be more precise, the thermal conductivity measurement was repeated 5 times at 20-minute intervals (to allow thermal stability), and the value reported in Table 3 is actually the average of the values obtained from the 5 experiments. To calibrate the device, the thermal conductivity of glycerol and water was measured at 20°C and the obtained values (0.274 W/m.K for glycerol and 0.586 W/m.K for water) were compared with the values in a valid source (0.285 W/m.K for glycerol and 0.598 W/m.K for water) [41]. The difference between the experimental results and the values reported in the ref. [41] was less than 3.9%. In addition, the density (ρ_{nf}) and specific heat ($c_{p,nf}$) of nanofluid were computed using the following equations [42]:

$$\rho_{nf} = (1-\varphi)\rho_w + \varphi\rho_p \quad (1)$$

$$c_{p,nf} = \frac{(1-\varphi)\rho_w c_{p,w} + \varphi\rho_p c_{p,p}}{\rho_{nf}} \quad (2)$$

where φ is the NA volume concentration and the subscripts nf, w and p stands for the nanofluid, water and NA. The density and specific heat of magnetite NAs are respectively 5200 kg/m^3 and 670 J/kg.K and the specific heat of water is 4179 J/kg.K [42].

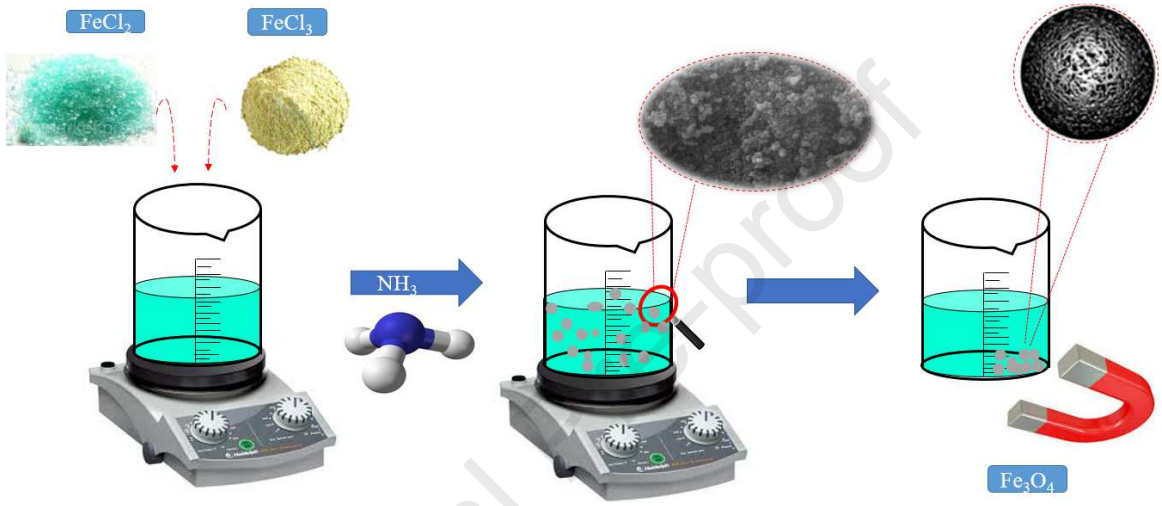

Fig. 4. Various steps of the preparation of water/magnetite nanofluid [40].

Table 3. Thermophysical properties of the prepared nanofluid (aqueous magnetite).

NA concentration (%)	Heat capacity (J/kg.K)	Thermal conductivity (W/m.K)	Density (kg/m^3)
0	4179.0	0.610	997.10
0.5	4089.39	0.695	1018.11
1	4003.40	0.873	1039.13
1.5	3920.83	0.917	1060.14
2	3841.46	0.961	1081.16

4. Energy and exergy formulation

The concept of the PVT system was developed to receive thermal energy and electrical energy simultaneously. Keeping this in mind, the present study is aimed to improve the thermal and electrical performances of the traditional plain serpentine tube collector by some

design modifications as discussed in section 2. The detailed formulation of energy, exergy, and electrical energy are presented in this section.

The thermal behavior of the PVT systems is characterized by its ability to produce total thermal energy with respect to the total solar energy received. This process is termed as thermal energy efficiency (η_{th}) of the PVT system [8]:

$$\eta_{th} = \frac{\dot{m}_{nf} c_{p,nf} \left(T_{nfo} - T_{nfi}\right)}{I_{sol} A_{pvm}} \times 100 \quad (3)$$

where T_{nfi}, T_{nfo}, $\dot{m}_{nf}$ and c_p respectively denote the inlet temperature, outlet temperature, mass flow rate, and specific heat capacity of nanofluid. In addition, I_{sol} and A_{pvm} are the striking radiation intensity and PV module area, respectively.

Similarly, the electrical behavior of the PVT system is characterized by its ability to produce electrical energy with respect to the total solar energy received. This process can be termed as electrical energy efficiency (η_{el}) of the PVT system [8]:

$$\eta_{el} = \frac{V_{pvm} I_{pvm} - \dot{E}_{elp}}{I_{sol} A_{pvm}} \times 100 \quad (4)$$

where I_{pvm} and V_{pvm} are respectively the output current and output voltage of the PV module. $\dot{E}_{elp}$ is the fluid pumping power which can be calculated as [43]:

$$\dot{E}_{elp} = \frac{\dot{m}_{nf} \Delta P}{\rho_{nf} \eta_p} \quad (5)$$

where ΔP and ρ_{nf} are the pressure drop and density of the nanofluid, respectively. Additionally, η_p is known as pump efficiency (=75%).

Thermal energy is characterized as low-grade energy whereas electrical energy is characterized as high-grade energy [8]. The conversion of electrical energy into thermal energy is possible with an approximate efficiency of 100% while the opposite behavior is not feasible. The PVT systems can be assessed and compared based on the overall energy efficiency which can be determined as [44]:

$$\eta_{ovth} = \eta_{th} + \frac{\eta_{el}}{0.36} \quad (6)$$

where 0.36 is the conversion coefficient of a coal-based power plant [44].

Exergy is one of the important applications of the second-law of thermodynamics and is characterized as the maximum work theoretically possible from a thermodynamic system. Accordingly, the exergy efficiency of the PVT system is characterized by the percentage of the maximum theoretically possible output that can be achieved as an actual desired output [35]. Therefore, it is important to assess the overall exergy scenario of the PVT systems which is the summation of the thermal exergy efficiency and electrical exergy efficiency (η_{elex}) [8]:

$$\eta_{ovex} = \eta_{thex} + \eta_{elex} \quad (7)$$

where η_{thex} is thermal exergy efficiency which is defined as the ratio of thermal exergy gain from the PVT system to the exergy of sun radiation [35, 45]:

$$\eta_{thex} = \frac{\dot{m}_{nf} c_{p,nf} \left(T_{nfo} - T_{nfi}\right) \left[1 - \frac{T_{amb} + 273}{T_{nfo} + 273}\right]}{I_{sol} A_{pvm} \alpha_{PV} \left[1 - \frac{4}{3}\left(\frac{T_{amb}}{T_{sun} \Upsilon}\right) + \frac{1}{3}\left(\frac{T_{amb}}{T_{sun} \Upsilon}\right)^4\right]} \times 100 \quad (8)$$

whereas η_{elex} is the electrical exergy efficiency expressed as the ratio of the electrical power gain from the PVT system to the exergy of sun radiation [31, 45]:

$$\eta_{elex} = \frac{V_{pvm} I_{pvm} - \dot{E}_{elp}}{I_{sol} A_{pvm} \alpha_{pv} \left[1 - \frac{4}{3}\left(\frac{T_{amb}}{T_{sun} \Upsilon}\right) + \frac{1}{3}\left(\frac{T_{amb}}{T_{sun} \Upsilon}\right)^4\right]} \times 100 \quad (9)$$

where T_{amb} and T_{sun} are the ambient temperature and sun temperature, respectively (≅5800 K). In addition, α_{pv} is the absorptivity of PV panel (=0.9) and Υ is the interaction factor, which is determined as follows [45]:

$$\Upsilon = \left(\frac{f_s \varepsilon_s}{f_c \varepsilon_c} \alpha_{pv}\right)^{1/4} \quad (10)$$

where ε_s and ε_c are the dilution factors for incoming solar radiation and PV panel emitted radiation, respectively. In addition, f_c is the geometric factor for solar collector and f_c is the geometric factor for solar radiation defined as the ratio of concentration of solar collector (C) to the maximum concentration of solar radiation at level of earth orbit (C_{max}).

5. Uncertainty analysis

To assess the accurate findings of the experimental study, the uncertainty of the used instruments must be considered. In this study, uncertainty analysis is carried out via the method established by Moffat [46] which identifies the uncertainty of the dependent variable (D) as a function of the independent variables (d_1, d_2, …, d_n) as expressed below:

$$\delta D = \sqrt{\left(\frac{\partial D}{\partial v d_1}\delta d_1\right)^2 + \left(\frac{\partial D}{\partial d_2}\delta d_2\right)^2 + \cdots + \left(\frac{\partial D}{\partial d_n}\delta d_n\right)^2} \quad (11)$$

In the above equation, δ represents the parameter's uncertainty. The outcomes demonstrated that in all the experiments conducted in the current contribution, the uncertainty of the parameters was less than 5.21%, which is a justifiable value. The details of the uncertainty calculations are given in "Appendix A".

6. Results and discussions

The performance of the three cases of the PVT system has been experimentally investigated in this work. The three cases of the PVT system have been studied under indoor solar testing facilities for a range of nanofluid flow rates (20-80 kg/hr) and NA concentration (0-2%). The base, 3-start rifled, and 6-start riffled PVT systems are compared with each other in terms of thermal and electrical performances at the mentioned flow rates and NA concentrations. The thermal energy performance of the three cases is discussed in the first sub-section whereas the second subsection explains the thermal exergy performance. The third subsection details

the electrical energy performance of the experimental arrangements. Finally, the electrical performance of the three cases under the cooling mode is also compared with those of the PV module without cooling.

6.1. Thermal energy and its related efficiency

Fig. 5 displays the thermal energy output gained by the three cases of the PVT system under the influence of the nanofluid flow rates and NA concentrations. It is witnessed that an increase in the flow rate and NA concentration results in a corresponding increase in the thermal energy output for all the three cases, i.e, the minimum thermal energy output has been observed at a flow rate and NA concentration of 20 kg/hr and 0% whereas the maximum value has been observed at 80 kg/hr and 2%. This is because the thermal energy gained by the PVT system depends on the magnitude of the flow rate and outlet fluid temperature. The increase in the flow rate directly influences the thermal energy gained by the PVT system whereas an increase in the flow rate has a negative effect on the outlet fluid temperature which results in a decrement of thermal energy gain. The effect of flow rates dominates the effect of outlet fluid temperature and resulted in an enhancement of thermal energy output with an increase in nanofluid flow rate (20-80 kg/hr). The reason for the enhancement in the thermal energy output with the increase in NA concentration from 0-2% at a given flow rate is due to the greater thermal conductivity of nanofluid at higher NA concentrations (see Table 3). The explained behavior of thermal energy output with the flow rates and NA concentrations is quantified below.

It is observed that for the base PVT system when the flow rate increased from 20-80 kg/hr at a 0% NA concentration, the thermal energy output increased by 21.9%. At a similar condition, this percentage improvement for the 3-start rifled, and 6-start rifled PVT systems has been evaluated to 24.2% and 24.4% respectively. For a similar increment in the flow rate

(20-80 kg/hr), at a 2% NA concentration, the thermal energy output enhancement for the base, 3-start rifled, and 6-strat rifled PVT systems is 21%, 24.8%, and 25.2% respectively. On the other hand, when NA concentration increased from 0-2% at a flow rate of 20 kg/hr, the thermal energy output increased by 17.1%, 19.9%, and 19.4% for the base, 3-start rifled, and 6-start rifled PVT system. For a similar increment in the NA concentration (0-2%), at a flow rate of 80 kg/hr, the thermal energy output enhancement for the base, 3-start rifled, and 6-start rifled PVT systems reaches 16.3%, 20.4%, and 20.2% respectively.

The crux of this investigation is to also directly compare the three cases of the PVT system. It is seen that the 6-start rifled PVT system has a higher thermal energy output as compared to the 3-start rifled and base PVT systems at any combinations of flow rate and NA concentration. It is seen that at a 2.0% and 80 kg/hr of NA concentration and flow rate, the 6-start rifled PVT system has gained thermal energy output of 39.7 W against 28.49 W and, 37.71W of the base and 3-start rifled PVT system. The 6-start rifled PVT system has a 39.3% and 5.3% higher thermal energy output than the base and 3-start rifled PVT systems at maximum flow rate (2 kg/hr) and NA concentration (2%). It is seen that when the base PVT system is modified into the 3-start rifled PVT system by adding 3 ribs, the thermal power output enhanced. Similarly, when the 3-start rifled PVT system is modified into the 6-start rifled PVT system by adding 6 rifled ribs, the thermal energy output further enhanced as quantified in the above discussions.

Two factors can be considered as the reasons for this behavior: first, the rifled tube has a higher heat transfer surface area compared to the plain tube, and secondly, due to the centrifugal force, the rifled tube entails the fluid rotation and, in consequence, the mixing of near-wall hot fluid with the cold fluid passing through the central region of the tube.

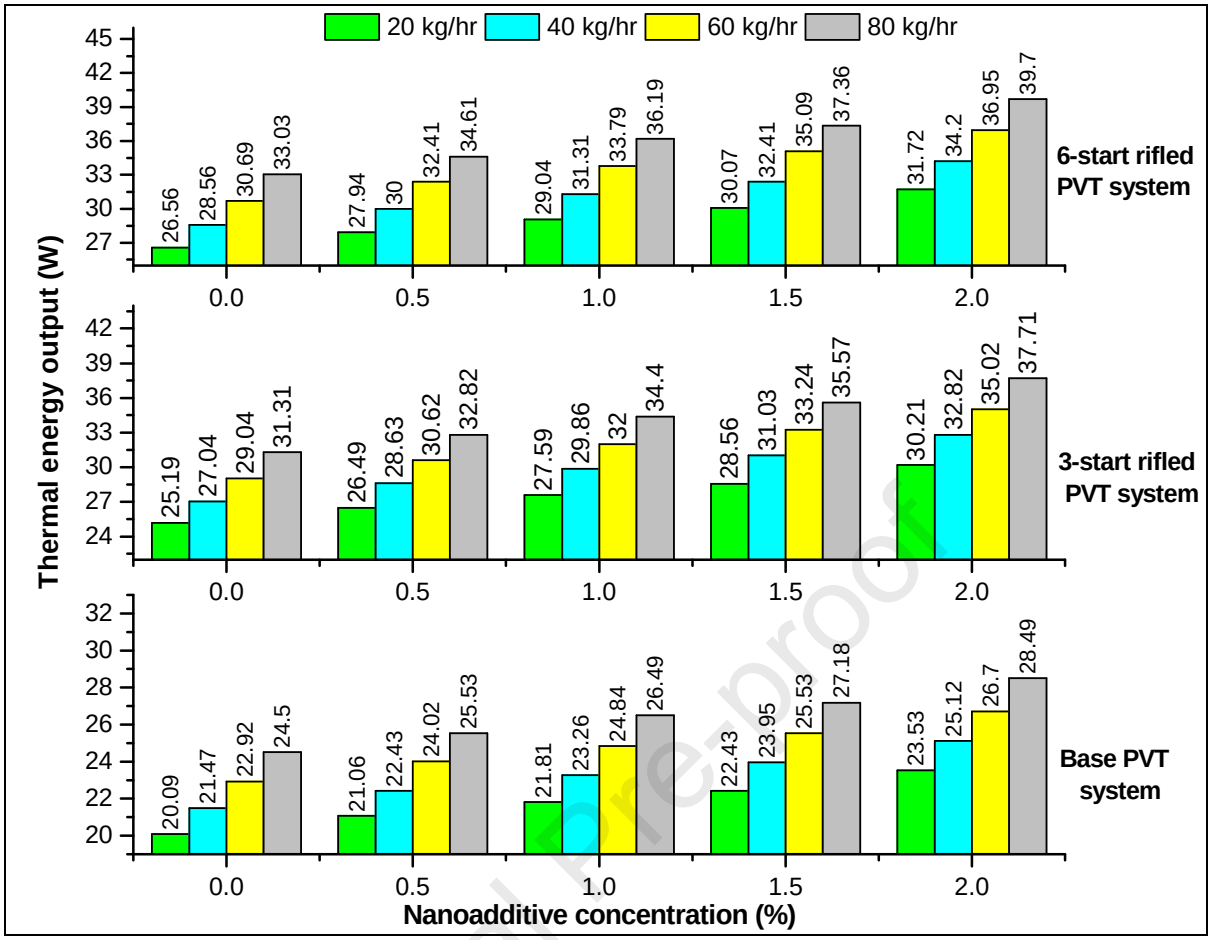

Fig. 5. Thermal energy output of the base, 3-start rifled, and 6-start rifled PVT systems at different flow rates and NA concentrations.

Table 4 and Fig. 6 show respectively the thermal energy efficiency and overall energy efficiency of the base, 3-start rifled, and 6-start rifled PVT systems for a range of nanofluid flow rates (20-80 kg/hr) and NA concentrations (0-2%). It is seen that both parameters increase with an increase in the flow rate and NA concentration. The minimum value of these parameters has been achieved at a combination of the NA concentration and flow rate of 0% and 20 kg/hr, while the maximum value is achieved at 2% and 80 kg/hr for all the three cases. The reasons for an increase in the value of thermal energy efficiency and overall energy efficiency with NA concentration and flow rate are similar to the case of thermal power.

In terms of quantitative value, it is evident from Table 4 and Fig. 6 that as the flow rate increased from 20-80 kg/hr at a 0% NA concentration, the thermal energy efficiency of the base, 3-start rifled, and 6-start rifled PVT system enhanced by 21.9%, 24.3%, and 24.4%, while these values are 21%, 24.8%, and 25.2% at a 2% NA concentration for a similar range of nanofluid flow rate. Again, the effect of increasing NA concentration at a given flow rate has also been observed in terms of thermal energy efficiency. It is seen that as the NA concentration increased from 0-2% at 20 kg/hr, the thermal energy efficiency of the base, 3-start rifled, and 6-start rifled PVT systems improved by 17.1%, 19.9%, and 19.4%, while these values are 16.3%, 20.4%, and 20.2% at the flow rate of 80 kg/hr for a similar range of NA concentration. On the other hand, when the three cases are compared with each other, it has been observed that the 6-start rifled PVT system achieved highest thermal energy efficiency of 57.7% against 41.4%, and 54.8% of the base and 3-start rifled PVT systems at the combination of maximum flow rate (80 kg/hr) and NA concentration (2%). This indicates that the 6-start rifled PVT system has 39.4%, and 5.3% higher thermal energy efficiency than the base and 3-start rifled PVT systems.

Coming to the overall energy efficiency behavior of the three cases of the PVT system, it has been observed that the base, 3-start rifled, and 6-start rifled PVT systems achieved an overall energy efficiency in the range of 64.66-78.04%, 72.66-92.08%, and 75.05-95.58% for the range of flow rate (20-80 kg/hr) and NA concentration (0-2%). These ranges suggest that the 6-start rifled PVT system has generated 22.5% and 3.8% higher overall energy efficiency when compared with the base, and 3-start rifled PVT system at a maximum flow rate (80 kg/hr) and NA concentration (2%). The reason for the dominance of the 6-start rifled PVT system over the base, and 3-start rifled PVT system in terms of thermal energy and overall energy efficiency is the same as explained for the case of thermal power.

412

413 **Table 4.** Thermal energy efficiency of the base, 3-start rifled, and 6-start rifled PVT systems at different flow rates and NA concentrations.

Mass flow rate ↓ (kg/hr)	Base PVT system					3-start rifled PVT system					6-start rifled PVT system				
NA concentrations → (%)	**0.0**	**0.5**	**1**	**1.5**	**2.0**	**0.0**	**0.5**	**1**	**1.5**	**2.0**	**0.0**	**0.5**	**1**	**1.5**	**2.0**
20	29.2	30.6	31.7	32.6	34.2	36.6	38.5	40.1	41.5	43.9	38.6	40.6	42.2	43.7	46.1
40	31.2	32.6	33.8	34.8	36.5	39.3	41.6	43.4	45.1	47.7	41.5	43.6	45.5	47.1	49.7
60	33.3	34.9	36.1	37.1	38.8	42.2	44.5	46.5	48.3	50.9	44.6	47.1	49.1	51	53.7
80	35.6	37.1	38.5	39.5	41.4	45.5	47.7	50.0	51.7	54.8	48.0	50.3	52.6	54.3	57.7

414

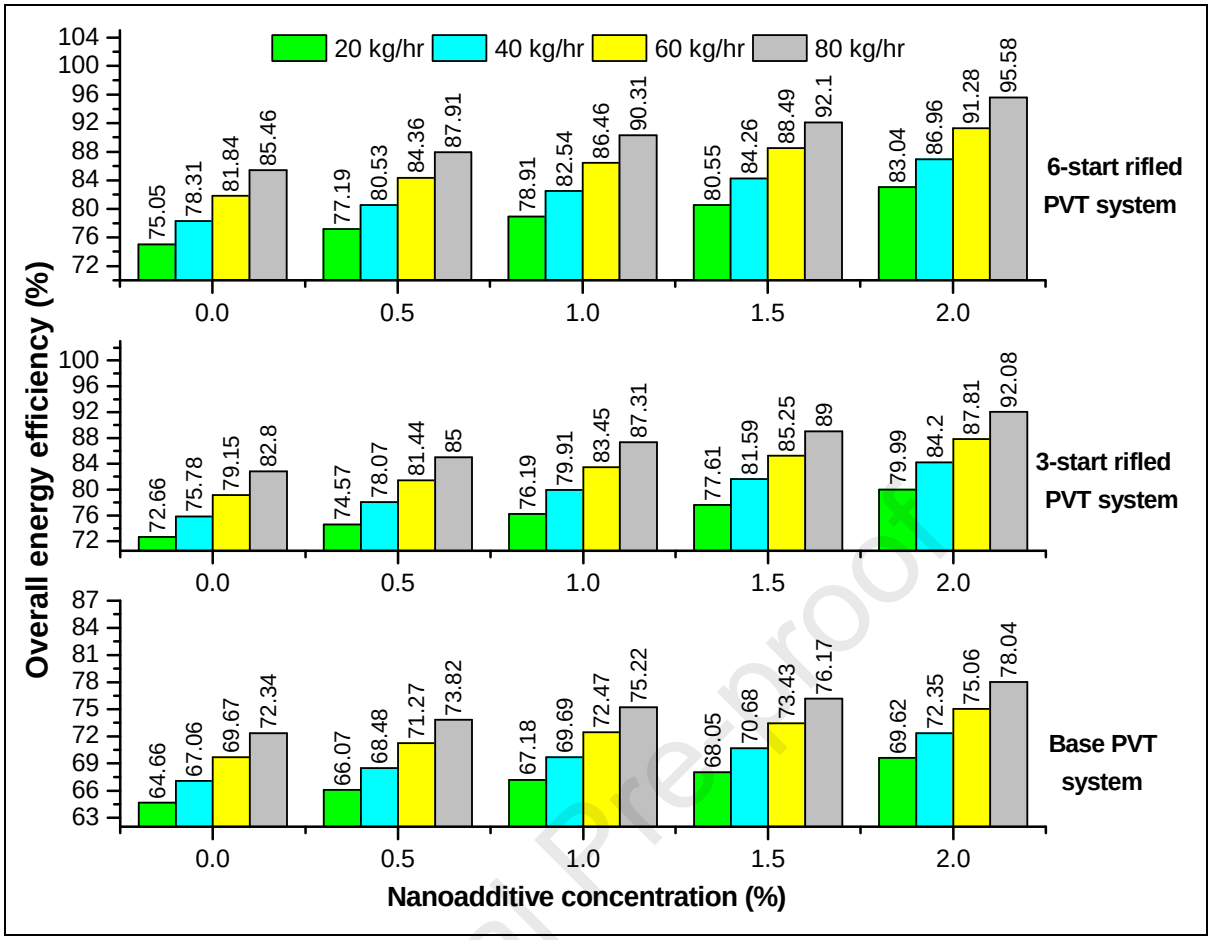

Fig. 6. Overall energy efficiency of the base, 3-start rifled, and 6-start rifled PVT system at different flow rates and NA concentrations.

6.2. Thermal exergy and its related efficiency

Figs. 7 and Table 5 display the thermal exergy output and thermal exergy efficiency gained by the three cases of the PVT system under the influence of the nanofluid flow rates and NA concentrations. It is shown that these three parameters for all the three cases increase with an increase in flow rates (20-80 kg/hr) and NA concentrations (0-2%). The reason for an increase in the value of these three parameters with an increase in the flow rate and NA concentration is the same as explained in the sub-section 6.1. The minimum value of these three parameters is achieved at a combination of NA concentration and flow rate of 0%, and 20 kg/hr, while the maximum is obtained for 2% and 80 kg/hr.

While observing the effect of increasing flow rate from 20-80 kg/hr at a given 0% NA concentration, the thermal exergy output for the base, 3-start rifled, and 6-start rifled PVT systems is enhanced by 44.4%, 55.5%, and 60.9% as shown in Fig. 7. On the other hand, at 2% NA concentration, these percentage enhancements are reported as 53.4%, 70.1%, and 76.5% under similar flow rate variations (20-80 kg/hr). Again, when the effect of increasing NA concentration (0-2%) is observed at a given flow rate of 20 kg/hr, the thermal exergy output for the base, 3-start rifled and 6-strat rifled PVT systems is enhanced respectively by 7.4%, 6.3%, and 6.2%, while these corresponding enhancements at 80 kg/hr are observed to be 14.1%, 16.3%, and 16.5%. Again, when these three cases are compared with each other, it has been found that the 6-start rifled PVT system has gained a highest thermal exergy output of 1.2 W against 0.89 W and 1.14 W of the base and 3-start rifled PVT systems at the maximum flow rate and NA concentration of 80 kg/hr and 2%. It can be said that the 6-start rifled PVT system has 34.8% and 5.3% higher thermal energy output than the base and 3-start rifled PVT systems.

The effect of increasing flow rate at a given NA concentration and vice versa in terms of thermal exergy efficiency is also evaluated in this investigation (Table 5). It is evidenced that as the flow rate increased from 20-80 kg/hr at a given NA concentration of 0%, the thermal exergy efficiency increased by 45.9%, 56.2%, and 60% for the base, 3-start rifled and 6-start rifled PVT systems, respectively, whereas at 2% NA concentration, these percentage enhancements are 53.6%, 72.3%, and 76.4%. Similarly, when NA concentration increased from 0-2% at a given flow rate of 20 kg/hr, the thermal exergy efficiency increased by 8.7%, 6.2%, and 5.4% for the base, 3-start rifled and 6-start rifled PVT systems, whereas at 80 kg/hr, these percentage enhancements are reported as 14.5%, 17.2%, and 16.2%. The comparison of the three cases shows that 6-start rifled PVT system has achieved thermal exergy efficiency of 3.07% against 2.29% and 2.93% of the base and 3-start rifled PVT

454 systems at 80 kg/hr and 2% NA concentration, which means that the 6-start rifled PVT
455 system has 34%, and 4.7% higher thermal exergy efficiency than the base and 3-start rifled
456 PVT systems.
457 Fig. 8 displays the overall exergy efficiency achieved by three cases of the PVT system at
458 different flow rates and NA concentrations. The base, 3-start rifled, and 6-start rifled PVT
459 systems gained an overall exergy efficiency in the range of 25.99-27.71%, 26.63-28.82%, and
460 26.96-29.36% for the range of flow rate (20-80 kg/hr), and NA concentration (0-2%). The
461 ranges discussed with the help of the Fig. 8 is a clear representation of an increasing overall
462 exergy efficiency with the increase in flow rate and NA concentration for all the three cases.
463 These ranges also suggest that the 6-strat rifled PVT system has the highest overall exergy
464 efficiency as compared to the other two configurations of the PVT system at any combination
465 of flow rate and NA concentration. It is seen that at 80 kg/hr of flow rate and 2% of NA
466 concentration, the 6-start rifled PVT system has generated 5.9%, and 1.9% higher overall
467 exergy efficiency than the base, and 3-start rifled PVT systems.
468

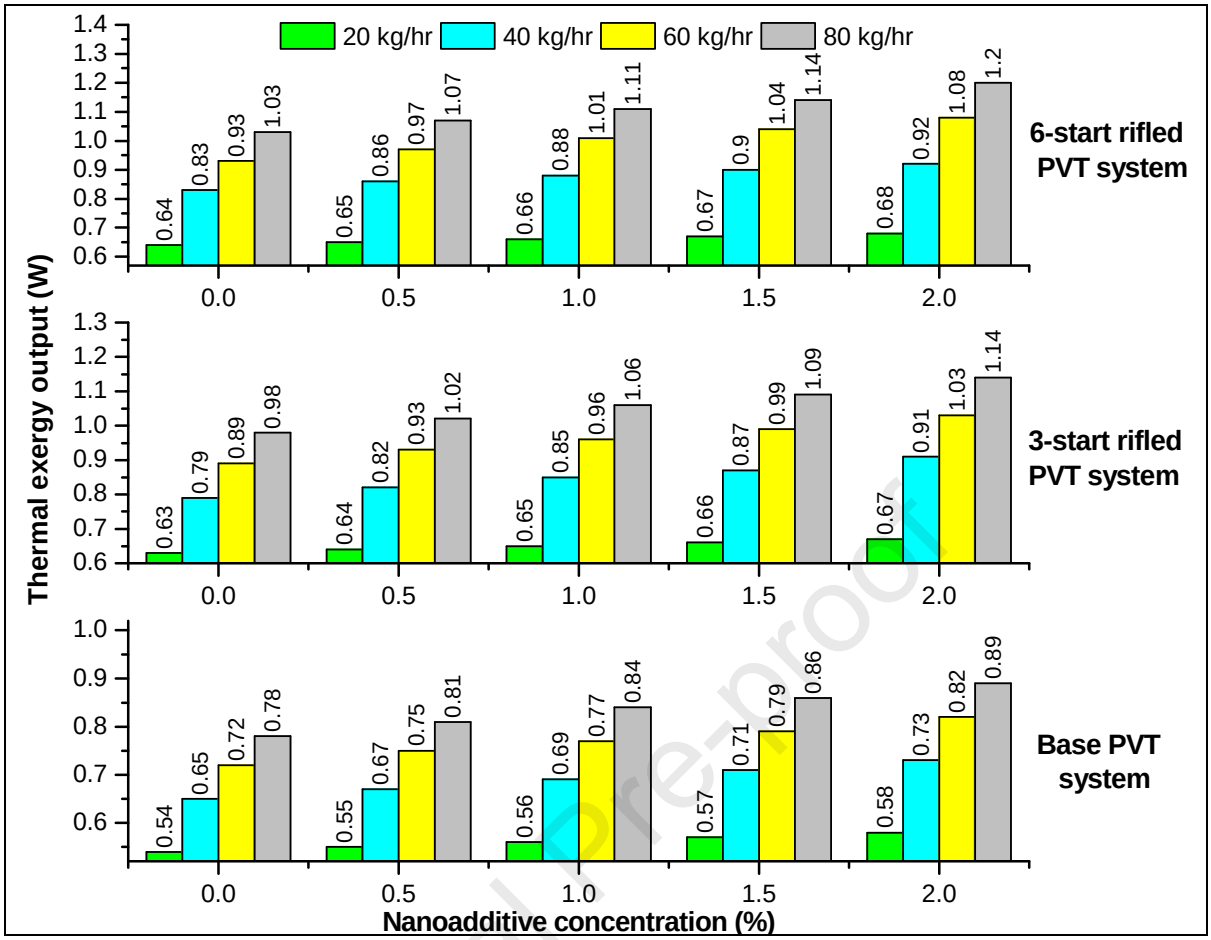

Fig. 7. Thermal exergy output of the base, 3-start rifled, and 6-start rifled PVT systems at different flow rates and NA concentrations.

473 **Table 5.** Thermal exergy efficiency of the base, 3-start rifled, and 6-start rifled PVT systems at different flow rates and NA concentrations.

Mass flow rate ↓ (kg/hr)	Base PVT system					3-start rifled PVT system					6-start rifled PVT system				
NA concentrations → (%)	**0.0**	**0.5**	**1**	**1.5**	**2.0**	**0.0**	**0.5**	**1**	**1.5**	**2.0**	**0.0**	**0.5**	**1**	**1.5**	**2.0**
20	1.37	1.42	1.44	1.46	1.49	1.6	1.67	1.67	1.68	1.7	1.65	1.68	1.7	1.72	1.74
40	1.67	1.72	1.77	1.81	1.87	2.01	2.1	2.17	2.22	2.33	2.12	2.19	2.26	2.31	2.38
60	1.84	1.91	1.98	2.01	2.1	2.27	2.38	2.47	2.53	2.64	2.4	2.5	2.59	2.66	2.76
80	2	2.08	2.15	2.19	2.29	2.5	2.6	2.73	2.79	2.93	2.64	2.74	2.85	2.92	3.07

474

475

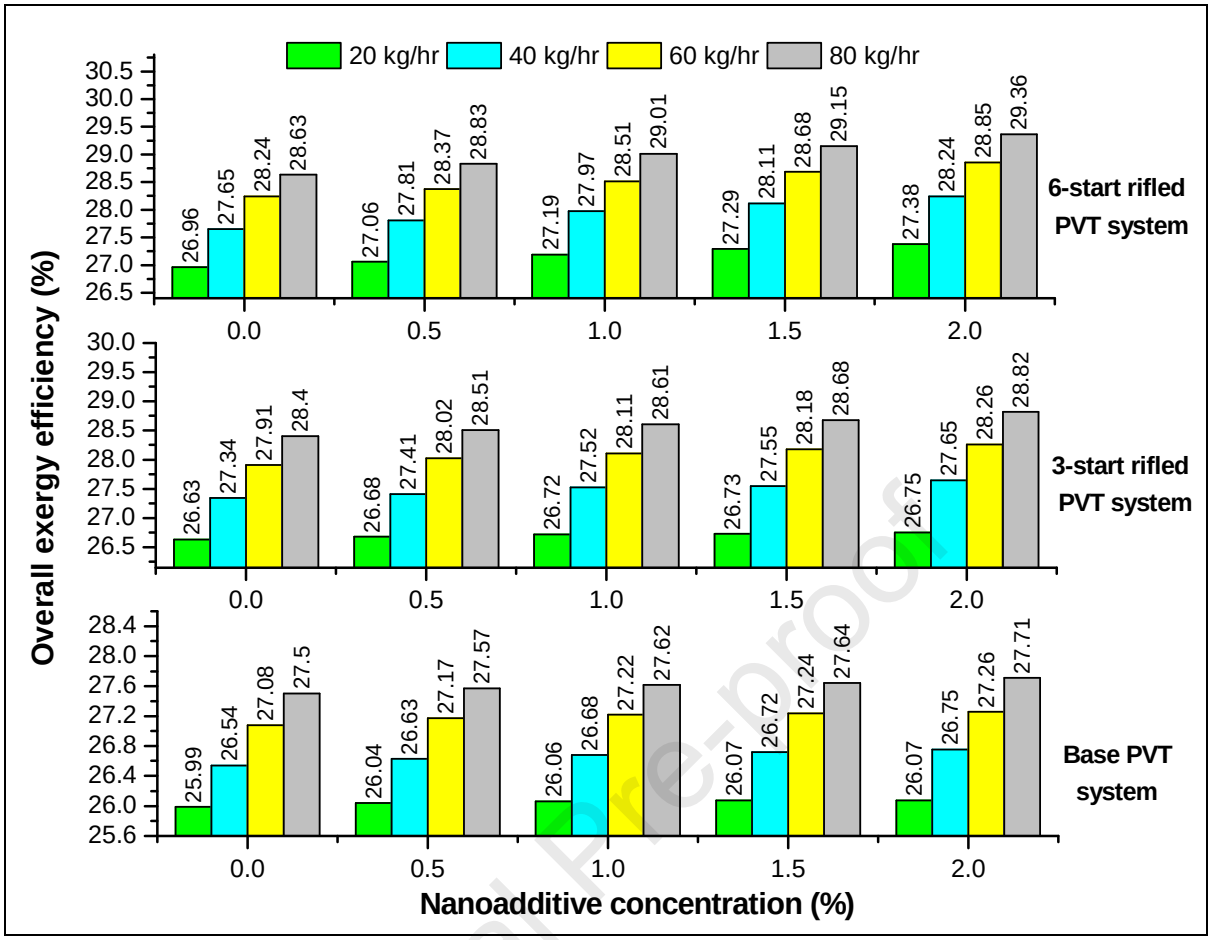

Fig. 8. Overall exergy efficiency of the base, 3-start rifled, and 6-start rifled PVT systems at different flow rates and NA concentration.

6.3. Electrical energy and its related efficiency

The concept of the PVT system was developed to reduce the operating temperature of the PV module as the high value of the PV module temperature deteriorates its electrical efficiency. So, in the present investigation, the temperature of the PV module and electrical power have been initially observed without cooling it by nanofluid. Under this condition, the value of the PV module temperature and electrical power have been observed as 346 K and 7.530 W. The investigation has been further extended to monitor the difference of the PV module temperature without cooling (T_{pv}) and the PV module temperature with cooling (T_{pvt}) for the three cases of the PVT system as shown in Fig. 9. The value of T_{pv}-T_{pvt} has been found in

the range of 23.56-32.77 K, 26.53-35.97 K, and 28.73-37.88K for the base, 3-start rifled, and 6-start rifled PVT systems respectively when the flow rate increased from 20-80 kg/hr and NA concentration from 0-2%. It is seen that the T_{pv}-T_{pvt} difference increases with the increase in flow rate and NA concentration for all the three cases. Fig. 9 further suggests that the maximum T_{pv}-T_{pvt} difference has been observed at 80 kg/hr and 2% NA concentration for all three cases and the 6-start rifled PVT system has the T_{pv}-T_{pvt} difference of 37.88 K which is 15.6%, and 5.3% higher than the base and 3-start rifled PVT systems, respectively. The reason for the higher T_{pv}-T_{pvt} difference for the 6-start rifled PVT system over the base and 3-start rifled PVT systems is due to the efficient heat transfer from the back of the PV module due to the 6 rifled ribs.

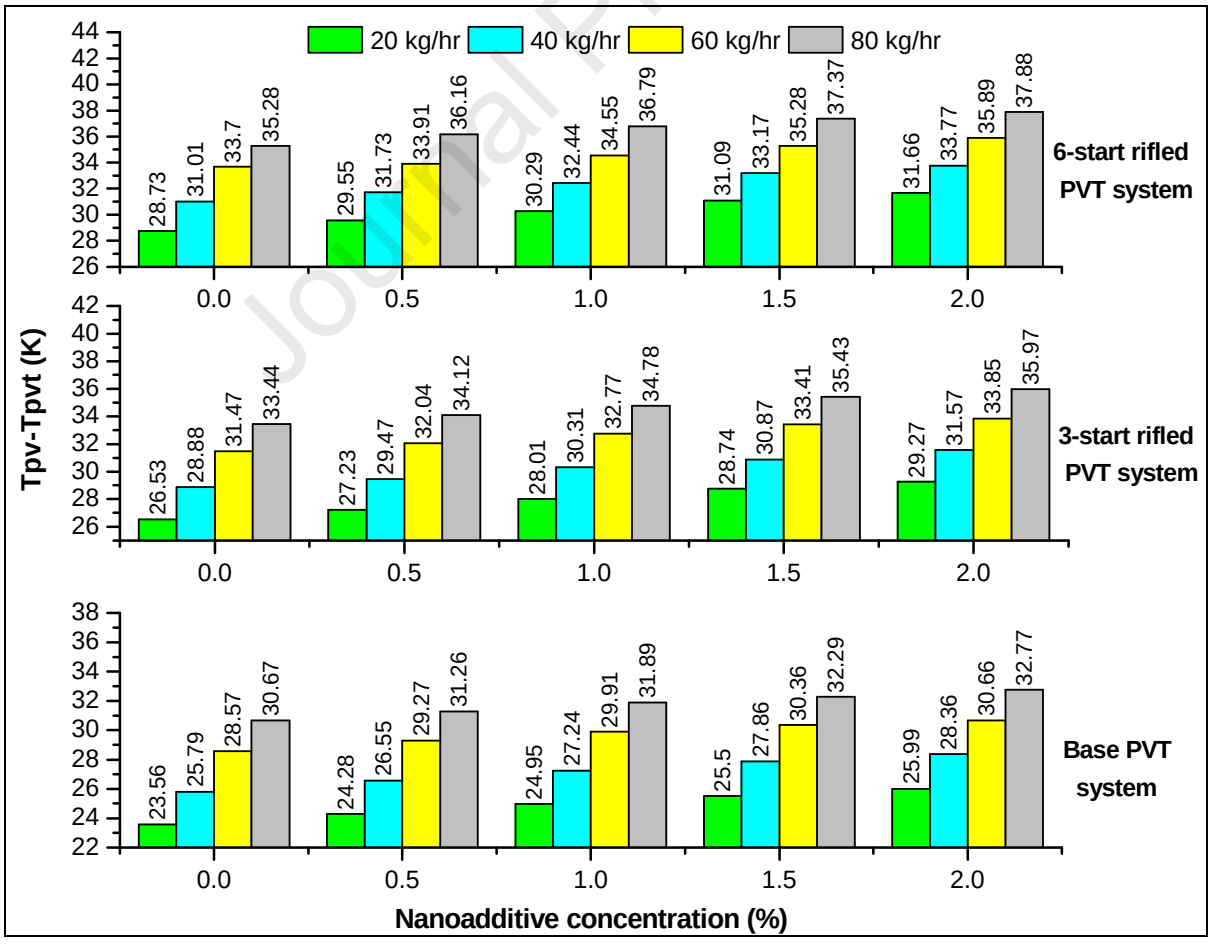

Fig. 9. T_{pv}-T_{pvt} difference of the base, 3-start rifled, and 6-start rifled PVT systems at different flow rates and NA concentrations.

Fig. 10 and Tables 13 and 14 display the electrical power, electrical energy efficiency, and electrical exergy efficiency achieved by the three cases of the PVT system under the influence of the increasing flow rate and NA concentration. It has been observed that these three parameters increase with an increase in the flow rate (20-80 kg/hr) at any given NA concentration. When the flow rate increased from 20-80 kg/hr at 0% NA concentration, the electrical power for the base, 3-start rifled and 6-start rifled PVT systems increased by 3.6%, 3.4%, and 2.8%, whereas at 2% NA concentration, these percentage enhancements are 3.4%, 3.3%, and 2.5%. The similar percentage enhancements are achieved in terms of the electrical energy efficiency and electrical exergy efficiency for the three cases at 0% and 2% NA concentration as the flow rate is increased from 20-80 kg/hr. The reason for the increase in the electrical efficiency at a given NA concentration when the flow rate is increased from 20-80 kg/hr is the higher efficient heat transfer. However, the behavior of the electrical parameters is not consistent when the utilized three cases are compared with each other as the NA concentration is increased from 0-2% at a given flow rate. This is because when the NA concentration increases, both viscosity and thermal conductivity of the nanofluid increases [24]. The increase in the viscosity results in high-pressure drop which causes high power consumption. On the other side, the increase in the thermal conductivity improves the PV cooling capacity and therefore increases the electrical power capacity of the PVT system. So, it is seen that for the base case when the NA concentration increased from 0-2% at 20 kg/hr, the electrical power, electrical energy efficiency, and electrical exergy efficiency decrease by 0.1%, whereas at 80 kg/hr, these parameters reduce by 0.3% because of higher power consumption at 2% NA concentration compared to at 0% NA concentration, which

outweighed the significance of higher conductivity. However, for the 3-start rifled PVT system, it has been observed that as the NA concentration increased from 0-2% at 20 kg/hr, the electrical power, electrical energy efficiency, and electrical exergy efficiency increased by 0.07% because of a better conductivity capacity of the nanofluid coupled with the effect of 3-start rifled ribs that resulted in a high electrical power from the PV module that outperformed the problem of power consumption. However, these three parameters for the 3-start rifled PVT system are decreased by 0.04% at 80 kg/hr because of the same reason as explained for the base PVT system. In the case of the 6-start rifled PVT system, the electrical power, electrical energy efficiency, and electrical exergy efficiency are increased by 1.3% at 20 kg/hr, and 1.1% at 80 kg/hr, as the NA concentration is increased from 0-2%. This is due to the fact that the nanofluid coupled with the 6-start rifled ribs results in a better PV cooling and hence a better electrical behavior.

Finally, this investigation shows that the maximum electrical power, electrical energy efficiency, and electrical exergy efficiency achieved in the case of base PVT system is 9.604 W, 13.958%, and 25.498% at 0% NA concentration, whereas the counterpart values for the 3-start rifled PVT system are 9.753 W,14.175%, and 25.498% at a 1% NA concentration, and for the 6-start rifled PVT system are 9.902 W, 14.398%, and 26.291% at a 2% NA concentration. All these maximum values for the three cases have been achieved at the flow rate of 80 kg/hr. This shows that the 6-start rifled PVT system has generated 3.1%, and 1.5% higher electrical power compared with the maximum value achieved by the base and 3-strat rifled PVT systems. A similar percentage enhancement has been observed for the 6-start rifled PVT system over the base and 3-start rifled PVT system in terms of electrical energy efficiency and electrical exergy efficiency.

The main objective of the PVT system is to enhance the electrical performance of the PV module. So, at the beginning of the study, the electrical power generated by the PV module

without cooling was observed and recorded as 7.530 W, and in the end, it is compared with the maximum electrical power generated by the three cases with cooling. So, the base, 3-start rifled, and 6-start rifled PVT system showed the percentage enhancement of 27.5%, 29.5%, and 31.5% of electrical power when compared with the PV module without cooling.

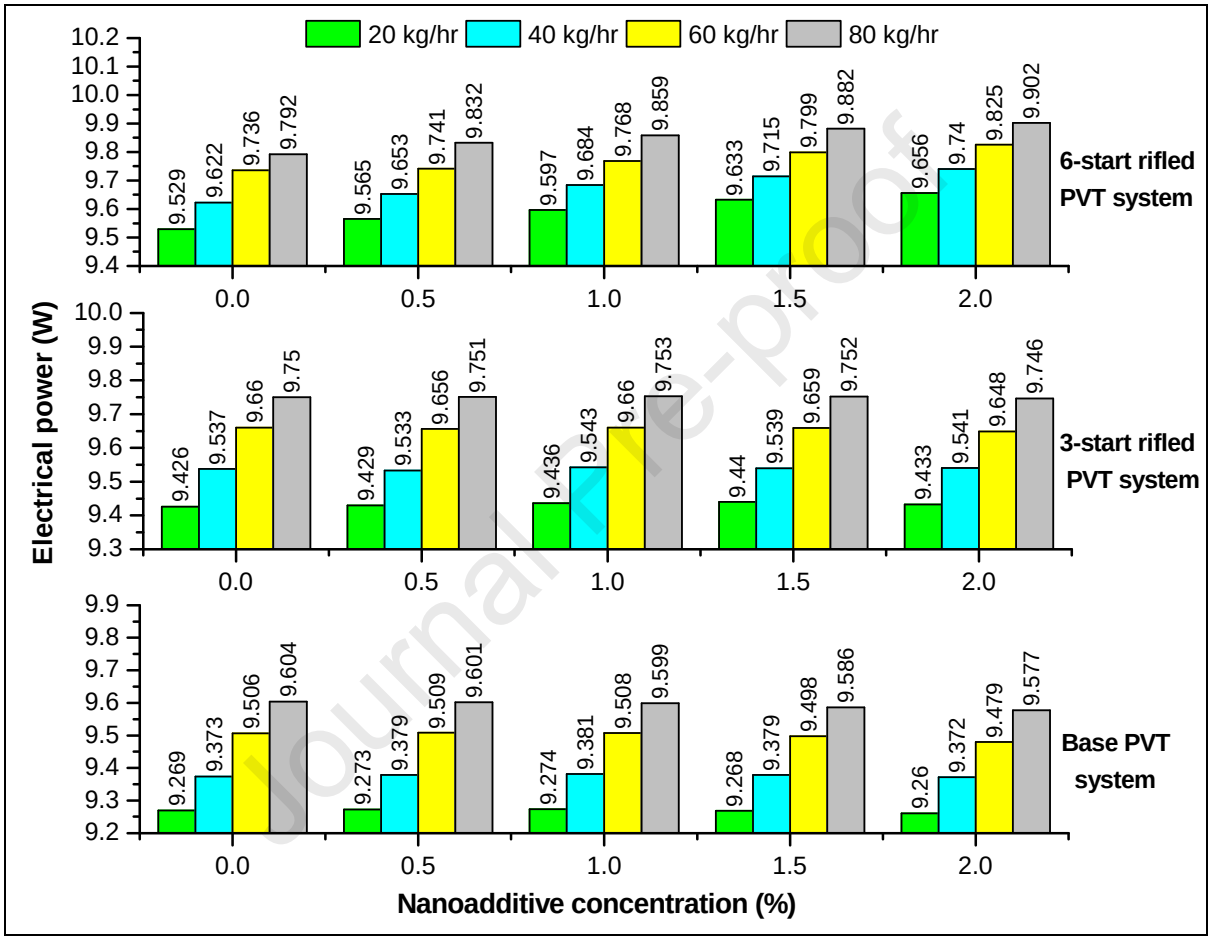

Fig. 10. Electrical power of the base, 3-start rifled, and 6-start rifled PVT systems at different flow rates and NA concentrations.

562

563

564 **Table 6.** Electrical energy efficiency of the base, 3-start rifled, and 6-start rifled PVT systems at different flow rates and NA concentrations.

Mass flow rate ↓ (kg/hr)	Base PVT system					3-start rifled PVT system					6-start rifled PVT system				
NA concentrations → (%)	**0.0**	**0.5**	**1**	**1.5**	**2.0**	**0.0**	**0.5**	**1**	**1.5**	**2.0**	**0.0**	**0.5**	**1**	**1.5**	**2.0**
20	13.471	13.477	13.478	13.470	13.458	13.700	13.703	13.713	13.719	13.710	13.850	13.903	13.949	14.001	14.035
40	13.623	13.631	13.634	13.632	13.620	13.860	13.855	13.870	13.863	13.867	13.985	14.030	14.075	14.121	14.157
60	13.816	13.820	13.819	13.804	13.777	14.039	14.033	14.039	14.038	14.022	14.152	14.158	14.197	14.243	14.280
80	13.958	13.953	13.951	13.932	13.919	14.171	14.173	14.175	14.174	14.165	14.233	14.291	14.329	14.364	14.393

565

566

567

568 **Table 7.** Electrical exergy efficiency of the base, 3-start rifled, and 6-start rifled PVT systems at different flow rates and NA concentrations.

Mass flow rate ↓ (kg/hr)	Base PVT system					3-start rifled PVT system					6-start rifled PVT system				
NA concentrations → (%)	**0.0**	**0.5**	**1**	**1.5**	**2.0**	**0.0**	**0.5**	**1**	**1.5**	**2.0**	**0.0**	**0.5**	**1**	**1.5**	**2.0**
20	24.609	24.619	24.623	24.607	24.585	25.027	25.034	25.052	25.026	25.047	25.298	25.395	25.481	25.576	25.637
40	24.887	24.901	24.908	24.902	24.882	25.321	25.312	25.338	25.326	25.333	25.547	25.628	25.71	25.795	25.861
60	25.239	25.246	25.246	25.217	25.168	25.647	25.635	25.647	25.645	25.616	25.85	25.862	25.934	26.017	26.085
80	25.498	25.489	25.487	25.451	25.428	25.887	25.89	25.894	25.892	25.876	26	26.104	26.175	26.237	26.291

7. Conclusions

In the present experimental investigation, three cases of the PVT system were investigated for various nanofluid flowrates and NA concentrations. These three cases are base PVT system, 3-start rifled PVT system, and 6-start rifled PVT system. It has been found that the increase in the flow rate and NA concentration from 20-80 kg/hr, and 0-2% increases the thermal performance of all three cases of the PVT system. Further, it has been found that the 6-start rifled PVT system has achieved a maximum of 22.5%, and 3.8% higher overall energy efficiency, and 5.9%, and 1.9% higher overall exergy efficiency than the base and 3-start rifled PVT system, respectively. In terms of electrical performance, the base and 3-start rifled PVT system, has achieved maximum performance at 0% and 1% NA concentrations at the flow rate of 80 kg/hr, whereas for the 6-start rifled PVT system, the maximum electrical performance has been achieved at 2% NA concentration and the flow rate of 80 kg/hr. Further, it has been concluded that the 6-start rifled PVT system has achieved 3.1% and 1.5% higher electrical power as compared with the base and 3-start rifled PVT systems. It is further found that the 6-start rifled PVT systems has achieved 31.5% higher electrical power with respect to the PV module without cooling as compared to its counterparts.

593 Appendix A: Details of uncertainty analysis

594 - Pumping power:

$$\overline{\dot{E}_{elp}} = f\left(\overline{\dot{m}_{nf}}, \overline{\Delta p}, \overline{\rho_{nf}}, \overline{\eta_p}\right)$$

$$u_{\dot{E}_{elp}} = f\left(u_{\dot{m}_{nf}}, u_{\Delta P}, u_{\rho_{nf}}, u_{\eta_p}\right) = \sqrt{\left(\frac{\delta \dot{E}_{elp}}{\delta \dot{m}_{nf}} u_{\dot{m}_{nf}}\right)^2 + \left(\frac{\delta \dot{E}_{elp}}{\delta \Delta P} u_{\Delta P}\right)^2 + \left(\frac{\delta \dot{E}_{elp}}{\delta \rho_{nf}} u_{\rho_{nf}}\right)^2 + \left(\frac{\delta \dot{E}_{elp}}{\delta \eta_p} u_{\eta_p}\right)^2}$$

$$\frac{u_{\dot{E}_{elp}}}{\dot{E}_{elp}} = \sqrt{\left(\frac{u_{\dot{m}_{nf}}}{\dot{m}_{nf}}\right)^2 + \left(\frac{u_{\Delta P}}{\Delta P}\right)^2 + \left(\frac{u_{\rho_{nf}}}{\rho_{nf}}\right)^2 + \left(\frac{u_{\eta_p}}{\eta_p}\right)^2} = 3.0\%$$

595

596 - Electrical energy efficiency:

$$\overline{\eta_{el}} = f\left(\overline{V_{pvm}}, \overline{I_{pvm}}, \overline{\dot{E}_{elp}}, \bar{I}_{sol}, \overline{A_{pvm}}\right)$$

$$u_{\eta_{el}} = f\left(u_{V_{pvm}}, u_{I_{pvm}}, u_{\dot{E}_{elp}}, u_{I_{sol}}, u_{A_{pvm}}\right) = \sqrt{\left(\frac{\delta \eta_{el}}{\delta V_{pvm}} u_{V_{pvm}}\right)^2 + \left(\frac{\delta \eta_{el}}{\delta I_{pvm}} u_{I_{pvm}}\right)^2 + \left(\frac{\delta \eta_{el}}{\delta \dot{E}_{elp}} u_{\dot{E}_{elp}}\right)^2 + \left(\frac{\delta \eta_{el}}{\delta I_{sol}} u_{I_{sol}}\right)^2 + \left(\frac{\delta \eta_{el}}{\delta A_{pvm}} u_{A_{pvm}}\right)^2}$$

$$\frac{u_{\eta_{el}}}{\eta_{el}} = \frac{100}{I_{sol} A_{pvm} \eta_{el}} \sqrt{\left(I_{pvm} u_{V_{pvm}}\right)^2 + \left(V_{pvm} u_{I_{pvm}}\right)^2 + \left(-u_{\dot{E}_{elp}}\right)^2 + \left(\frac{\dot{E}_{elp} - V_{pvm} I_{pvm}}{I_{sol}} u_{I_{sol}}\right)^2 + \left(\frac{\dot{E}_{elp} - V_{pvm} I_{pvm}}{A_{pvm}} u_{A_{pvm}}\right)^2} = 5.19\%$$

597

598 - Thermal energy efficiency:

$$\overline{\eta_{th}} = f\left(\overline{\dot{m}_{nf}}, \overline{c_{p,nf}}, \overline{T_{nfo}}, \overline{T_{nfi}}, \bar{I}_{sol}, \overline{A_{pvm}}\right)$$

$$u_{\eta_{th}} = f\left(u_{\dot{m}_{nf}}, u_{c_{p,nf}}, u_{T_{nfo}}, u_{T_{nfi}}, u_{I_{sol}}, u_{A_{pvm}}\right)$$

$$= \sqrt{\left(\frac{\delta\eta_{th}}{\delta\dot{m}_{nf}}u_{\dot{m}_{nf}}\right)^2 + \left(\frac{\delta\eta_{th}}{\delta c_{p,nf}}u_{c_{p,nf}}\right)^2 + \left(\frac{\delta\eta_{th}}{\delta T_{nfo}}u_{T_{nfo}}\right)^2 + \left(\frac{\delta\eta_{th}}{\delta T_{nfi}}u_{T_{nfi}}\right)^2 + \left(\frac{\delta\eta_{th}}{\delta I_{sol}}u_{I_{sol}}\right)^2 + \left(\frac{\delta\eta_{th}}{\delta A_{pvm}}u_{A_{pvm}}\right)^2}$$

$$\frac{u_{\eta_{th}}}{\eta_{th}} = \sqrt{\left(\frac{u_{\dot{m}_{nf}}}{\dot{m}_{nf}}\right)^2 + \left(\frac{u_{c_{p,nf}}}{c_{p,nf}}\right)^2 + \left(\frac{u_{T_{nfo}}}{T_{nfo} - T_{nfi}}\right)^2 + \left(\frac{u_{T_{nfi}}}{T_{nfo} - T_{nfi}}\right)^2 + \left(\frac{u_{I_{sol}}}{I_{sol}}\right)^2 + \left(\frac{u_{A_{pvm}}}{A_{pvm}}\right)^2} = 4.43\%$$

599

600 - Electrical exergy efficiency:

$$\overline{\eta_{elex}} = f\left(\overline{V_{pvm}}, \overline{I_{pvm}}, \overline{\dot{E}_{elp}}, \bar{I}_{sol}, \overline{A_{pvm}}, \overline{T_{amb}}\right)$$

$$u_{\eta_{elex}} = f\left(u_{V_{pvm}}, u_{I_{pvm}}, u_{\dot{E}_{elp}}, u_{I_{sol}}, u_{A_{pvm}}, u_{T_{amb}}\right)$$

$$= \sqrt{\left(\frac{\delta\eta_{elex}}{\delta V_{pvm}}u_{V_{pvm}}\right)^2 + \left(\frac{\delta\eta_{elex}}{\delta I_{pvm}}u_{I_{pvm}}\right)^2 + \left(\frac{\delta\eta_{elex}}{\delta\dot{E}_{elp}}u_{\dot{E}_{elp}}\right)^2 + \left(\frac{\delta\eta_{elex}}{\delta I_{sol}}u_{I_{sol}}\right)^2 + \left(\frac{\delta\eta_{elex}}{\delta A_{pvm}}u_{A_{pvm}}\right)^2 + \left(\frac{\delta\eta_{elex}}{\delta T_{amb}}u_{T_{amb}}\right)^2}$$

$$\frac{u_{\eta_{elex}}}{\eta_{elex}} =$$

$$\frac{100}{I_{sol}A_{pvm}\eta_{el}\left[1-\frac{4}{3}\left(\frac{T_{amb}}{T_{sun}}\right)+\frac{1}{3}\left(\frac{T_{amb}}{T_{sun}}\right)^4\right]}\sqrt{\left(I_{pvm}u_{V_{pvm}}\right)^2+\left(V_{pvm}u_{I_{pvm}}\right)^2+\left(-u_{\dot{E}_{elp}}\right)^2+\left(\frac{\dot{E}_{elp}-V_{pvm}I_{pvm}}{I_{sol}}u_{I_{sol}}\right)^2+\left(\frac{\dot{E}_{elp}-V_{pvm}I_{pvm}}{A_{pvm}}u_{A_{pvm}}\right)^2+\left[\left(\frac{-4T_{sun}^3+12T_{amb}^3}{3T_{sun}^4}\right)u_{T_{amb}}\right]^2}$$

$$= 5.21\%$$

601

602 - Thermal exergy efficiency:

$$\overline{\eta_{thex}} = f\left(\overline{\dot{m}_{nf}}, \overline{c_{p,nf}}, \overline{T_{nfo}}, \overline{T_{nfi}}, \bar{I}_{sol}, \overline{A_{pvm}}, \overline{T_{amb}}\right)$$

$$u_{\eta_{thex}} = f\left(u_{\dot{m}_{nf}}, u_{c_{p,nf}}, u_{T_{nfo}}, u_{T_{nfi}}, u_{I_{sol}}, u_{A_{pvm}}, u_{T_{amb}}\right)$$

$$= \sqrt{\left(\frac{\delta\eta_{thex}}{\delta\dot{m}_{nf}}u_{\dot{m}_{nf}}\right)^2+\left(\frac{\delta\eta_{thex}}{\delta c_{p,nf}}u_{c_{p,nf}}\right)^2+\left(\frac{\delta\eta_{thex}}{\delta T_{nfo}}u_{T_{nfo}}\right)^2+\left(\frac{\delta\eta_{thex}}{\delta T_{nfi}}u_{T_{nfi}}\right)^2+\left(\frac{\delta\eta_{thex}}{\delta I_{sol}}u_{I_{sol}}\right)^2+\left(\frac{\delta\eta_{thex}}{\delta A_{pvm}}u_{A_{pvm}}\right)^2+\left(\frac{\delta\eta_{thex}}{\delta T_{amb}}u_{T_{amb}}\right)^2}$$

$$\frac{u_{\eta_{thex}}}{\eta_{thex}} = \sqrt{\left(\frac{u_{\dot{m}_{nf}}}{\dot{m}_{nf}}\right)^2+\left(\frac{u_{c_p,nf}}{c_{p,nf}}\right)^2+\left(\frac{u_{T_{nfo}}}{T_{nfo}-T_{nfi}}\right)^2+\left(\frac{u_{T_{nfi}}}{T_{nfo}-T_{nfi}}\right)^2+\left(\frac{u_{I_{sol}}}{I_{sol}}\right)^2+\left(\frac{u_{A_{pvm}}}{A_{pvm}}\right)^2+\left(\frac{\delta\eta_{thex}}{\delta T_{amb}}\frac{u_{T_{amb}}}{\eta_{thex}}\right)^2} = 4.67\%$$

603

References

[1] C. Zou, Q. Zhao, G. Zhang, B. Xiong, Energy revolution: From a fossil energy era to a new energy era, Nat. Gas Ind. B 3 (2016) 1–11

[2] M. Ameri, M.M. Mahmoudabadi, A. Shahsavar, An experimental study on a PV/T air collector with direct coupling of fans and panels, Energy Sources, Part A 34 (2012) 929–947.

[3] M.H. Esfe, M.H. Kamyab, M. Valadkhani, Application of nanofluids and fluids in photovoltaic thermal system: An updated review, Solar Energy 199 (2020) 796–818.

[4] A. Shahsavar, M. Salmanzadeh, M. Ameri, P. Talebizadeh, Energy saving in buildings by using the exhaust and ventilation air for cooling of photovoltaic panels, Energy and Buildings 43 (2011) 2219–2226.

[5] M. Khaki, A. Shahsavar, S. Khanmohammadi, Scenario-Based Multi-Objective Optimization of an Air- Based Building-Integrated Photovoltaic/Thermal System, Journal of solar Energy Engineering 140 (2017) 011003.

[6] M. Wolf, Performance analysis of combined heating and photovoltaic power systems for residences, Energy Conversion 16 (1976)79–90.

[7] W. Gao, H. Moayedi, A. Shahsavar, The feasibility of genetic programming and ANFIS in prediction energetic performance of a building integrated photovoltaic thermal (BIPVT) system, Solar Energy 183 (2019) 293-305.

[8] Z.X. Li, A. Shahsavar, A.A.A. Al-Rashed, R. Kalbasi, M. Afrand, P. Talebizadehsardari, Multi-objective energy and exergy optimization of different configurations of hybrid earth-air heat exchanger and building integrated photovoltaic/thermal system, Energy Conversion and Management 195 (2019) 1098–1110.

[9] S. Khanmohammadi, A. Shahsavar, Energy analysis and multi-objective optimization of a novel exhaust air heat recovery system consisting of an air-based building integrated photovoltaic/ thermal system and a thermal wheel, Energy Conversion and Management 172 (2018) 595–610.

[10] M. Farshchimonfared, J.I. Bilbao, A.B. Sproul, Channel depth, air mass flow rate and air distribution duct diameter optimization of photovoltaic thermal (PV/T) air collectors linked to residential buildings, Renewable Energy 76 (2015) 27–35.

[11] J.C. Mojumder, W.T. Chong, H.W. Ong, K.Y. Leong, A.A. Mamoon, An experimental investigation on performance analysis of air type photovoltaic thermal collector system integrated with cooling fins design, Energy Building 130 (2016) 272–285.

[12] A. Fudholi, M. Zohri, G.L. Jin, A. Ibrahim, C.H. Yen, M.Y. Othman, M.H. Ruslan, K. Sopian, Energy and exergy analyses of photovoltaic thermal collector with ∇-groove, Solar Energy 159 (2018)742–750.

[13] F. Hussain, M.Y.H. Othman, B. Yatim, H. Ruslan, K. Sopian, Z. Anuar, S. Khairuddin, An improved design of photovoltaic/thermal solar collector, Solar Energy 122 (2015) 885–891.

[14] A.M. Elsaf, P. Gandhidasan, Comparative study of double-pass flat and compound parabolic concentrated photovoltaic–thermal systems with and without fins, Energy Conversion and Management 98 (2015) 59–68.

[15] M. Slimani, M. Amirat, KuruczI, S. Bahria, A. Hamidat, W.B. Chaouch, A detailed thermal-electrical model of three photovoltaic/thermal (PV/T) hybrid air collectors and photovoltaic (PV) module: Comparative study under Algiers climatic conditions, Energy Conversion and Management 133 (2017) 458–476.

[16] P. Ooshaksaraei, K. Sopian, S.H. Zaidi, R. Zulkifli, Performance of four air-based photovoltaic thermal collectors configurations with bifacial solar cells, Renewable Energy 102 (2017) 279–293.

[17] A. Shahsavar, M. Ameri, Experimental investigation and modelling of a direct coupled PV/T air collector, Solar Energy 84 (2010)1938–1958.

[18] A. Shahsavar, M. Ameri, M. Gholampour, Energy and exergy analysis of a photovoltaic- thermal collector with natural airflow, Journal of solar Energy Engineering 134 (2012) 011014–2.

[19] E.E. Bajestan, M.C. Moghadam, H.N.W. Daungthongsuk, S. Wongwises, Experimental and numerical investigation of nanofluids heat transfer characteristics for application in solar heat exchangers, International Journal of Heat and Mass Transfer 92 (2016)1041–1052.

[20] T. Sokhansefat, A.B. Kasaeian, F. Kowsary, Heat transfer enhancement in parabolic trough collector tube using Al_2O_3/synthetic oil nanofluid, Renewable and Sustainable Energy Reviews 33 (2014) 636–644.

[21] W.I. Liu, J. Alsarraf, A. Shahsavar, M. Rostamzadeh, M. Afrand, T.K. Nguyen, Impact of oscillating magnetic field on the thermal-conductivity of water-Fe_3O_4 and water-Fe_3O_4/CNT ferro-fluids: Experimental study, Journal of Magnetism and Magnetic Materials 484 (2019) 258-265.

[22] A. Shahsavar, S. Khanmohammadi, D. Toghraie, H. Salihepour, Experimental investigation and develop ANNs by introducing the suitable architectures and training algorithms supported by sensitivity analysis: Measure thermal conductivity and viscosity for liquid paraffin based nanofluid containing Al_2O_3 nanoparticles, Journal of Molecular Liquids 276 (2019) 850-860.

[23] A. Shahsavar, S. Khanmohammadi, A. Karimipour, M. Goodarzi, A novel comprehensive experimental study concerned synthesizes and prepare liquid paraffin-Fe_3O_4 mixture to develop models for both thermal conductivity & viscosity: A new approach of GMDH type of neural network, International Journal of Heat and Mass Transfer 131 (2019) 432-441.

[24] A. Shahsavar, M.R. Salimpour, M. Saghafian, M.B. Shafii, Effect of magnetic field on thermal conductivity and viscosity of a magnetic nanofluid loaded with carbon nanotubes, Journal of Mechanical Science and Technology 30 (2016) 809-815.

[25] F. Yazdanifard, M. Ameri. E. Ebrahimnia-Bajestan, Performance of nanofluid based photovoltaic/thermal systems: a review, Renewable and Sustainable Energy Reviews 76 (2017) 323–352.

[26] M. Moradgholi, S.M. Nowee, A. Farzaneh, Experimental study of using Al2O3/methanol nanofluid in a two phase closed thermosyphon (TPCT) array as a novel photovoltaic/thermal system, Solar Energy 164 (2018) 243–250.

[27] M. Sardarabadi, M. Passandideh-Fard, Experimental and numerical study of metal-oxides/water nanofluids as coolant in photovoltaic thermal systems (PVT), Solar Energy Materials and Solar Cells 157(2016) 533–542.

[28] N. Purohit, S. Jakhar, P. Gullo, M.S. Dasgupta, Heat transfer and entropy generation analysis of alumina/water nanofluid in a flat plate PV/T collector under equal pumping power comparison criterion, Renewable Energy 120 (2018)14–22.

[29] A.H.A. Al-Waeli, H.A. Kazem, J.H. Yousif, M.T. Chaichan, K. Sopian, Mathematical and neural network modeling for predicting and analyzing of nanofluid-nano PCM photovoltaic thermal systems performance, Renewable Energy 145 (2020) 963–980.

[30] A. Hassan, A. Wahab, M.A. Qasim, M.M. Janjua, M.A. Ali, H.M. Ali, T.R. Jadoon, E. Ali, A. Raza, N. Javaid, Thermal management and uniform temperature regulation of photovoltaic modules using hybrid phase change materials-nanofluids system, Renewable Energy 145 (2020) 282–293.

[31] A.H.A. Al-Waeli, A. Hussein, Kazem, M.T. Chaichan, K. Sopian, Experimental investigation of using nano-PCM/nanofluid on a photovoltaic thermal system (PVT): Technical and economic study, Thermal Science and Engineering Progress 11 (2019) 213–230.

[32] A. Fudholi, N.F.M. Razali, M.H. Yazdi, A. Ibrahim, M.H. Ruslan, M.Y. Othman, K. Sopian, TiO2/water-based photovoltaic thermal (PVT) collector: Novel theoretical approach, Energy 183 (2019) 305–314.

[33] M. Sardarabadi, M. Hosseinzadeh, A. Kazemian, M. Pasandideh-Fard, Experimental investigation of the effects of using metal-oxides/water nanofluids on a photovoltaic thermal system (PVT) from energy and exergy viewpoints, Energy Conversion and Management 138 (2017) 682-695.

[34] M. Sardarabadi, M. Passandideh-Fard, H.S. Zeinali, Experimental investigation of the effects of silica/water nanofluid on PV/T (photovoltaic thermal units), Energy 66 (2014)264–272.

[35] S. Aberoumand, S. Ghamari, B. Shabani, Energy and exergy analysis of a photovoltaic thermal (PV/T) system using nanofluids: An experimental study, Solar Energy165 (2018)167–177.

[36] M. Hosseinzadeh, M. Sardarabadi, M. Pasandideh-Fard, Energy and exergy analysis of nanofluid based photovoltaic thermal system integrated with phase change material, Energy147 (2018) 636– 647.

[37] Q. Yu, A. Romagnoli, R. Yang, D. Xie, C. Liu, Y. Ding, Y. Li, Numerical study on energy and exergy performances of a microencapsulated phase change material slurry based photovoltaic/thermal module, Energy Conversion and Management 183 (2019) 708–720.

[38] Y. Khanjari, F. Pourfayaz, A.B. Kasaeian, Numerical investigation on using of nanofluid in a water-cooled photovoltaic thermal system, Energy Conversion and Management 122(2016) 263–278.

[39] Y.S. Long, E.Y. Wang, T.C. Wu, C. Lien, Evaluation emerging PV Performance Rating under indoor lighting simulator, 2018 IEEE 7th World Conference on Photovoltaic Energy Conversion (WCPEC) (A Joint Conference of 45th IEEE PVSC, 28th PVSEC & 34th EU PVSEC).

[40] A. Shahsavar, M. Eisapour, P. Talebizadehsardari, Experimental evaluation of novel photovoltaic/thermal systems using serpentine cooling tubes with different cross-sections of circular, triangular and rectangular, Energy 208 (2020) 118409.

[41] https://webbook.nist.gov/

[42] M. Sheikholeslami, D.D. Ganji, Ferrohydrodynamic and magnetohydrodynamic effects on ferrofluid flow and convective heat transfer, Energy 75 (2014) 400-410.

[43] J. Yazdanpanahi, F. Sarhaddi, M. Mahdavi Adeli, Experimental investigation of exergy efficiency of a solar photovoltaic thermal (PVT) water collector based on exergy losses, Solar Energy 118 (2015)197–208.

[44] A.S. Joshi, A. Tiwari, G.N. Tiwari, I. Dincer, B.V. Reddy, Performance evaluation of a hybrid photovoltaic thermal (PV/T)(glass-to-glass) system, International Journal of Thermal Sciences 48 (2009) 154-164.

[45] V. Badescu, How much work can be extracted from diluted solar radiation?, Solar Energy 170 (2018) 1095-1100.

749 [46] R. Moffat, Describing the uncertainties in experimental results, Experimental
750 Thermal and Fluid Science 1 (1988) 3-17.

Highlights:

- Energetic and exergetic performances of a nanofluid-based PVT unit are assessed.
- The unit is equipped with a sheet-and-rifled serpentine tube collector.
- Aqueous suspension of magnetite nanoparticles is considered as coolant.
- Energetic and exergetic performances of the unit intensify with boosting φ and $\dot{m}_{nf}$.
- Overall energy and exergy efficiencies of rifled PVT unit is better than base unit.

Declaration of interests

☒ The authors declare that they have no known competing financial interests or personal relationships that could have appeared to influence the work reported in this paper.

☐The authors declare the following financial interests/personal relationships which may be considered as potential competing interests: